ACS APPLIED MATERIALS & INTERFACES

Research Article

www.acsami.org

Ultrathin Single-Walled Carbon Nanotube Network Framed Graphene Hybrids

Rui Wang,[†] Tu Hong,[‡] and Ya-Qiong Xu*[,†,‡]

[†]Department of Physics and Astronomy and [‡]Department of Electrical Engineering and Computer Science, Vanderbilt University, Nashville, Tennessee 37235, United States

Supporting Information

ABSTRACT: Graphene and single-walled carbon nanotubes (SWNTs) have shown superior potential in electronics and optoelectronics because of their excellent thermal, mechanical, electronic, and optical properties. Here, a simple method is developed to synthesize ultrathin SWNT−graphene films through chemical vapor deposition. These novel two-dimensional hybrids show enhanced mechanical strength that allows them to float on water without polymer supporting layers. Characterizations by Raman spectroscopy and transmission electron microscopy indicate that SWNTs can interlace as a concrete backbone for the subsequent growth of monolayer graphene. Optical and electrical transport measurements further show that SWNT−graphene hybrids inherit high optical transparency and superior electrical conductivity from monolayer graphene. We also explore the local optoelectronic properties of SWNT−graphene hybrids through spatially resolved photocurrent microscopy and find that the interactions between SWNTs and graphene can induce a strong photocurrent response in the areas where SWNTs link different graphene domains together. These fundamental studies may open a door for engineering optoelectronic properties of SWNT−graphene hybrids by controlling the morphologies of the SWNT frames.

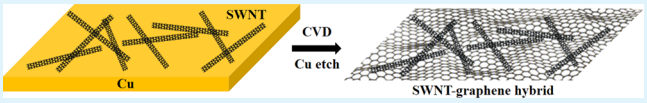

KEYWORDS: *CVD, graphene, single-walled carbon nanotube, photocurrent*

1. INTRODUCTION

Graphene and carbon nanotubes (CNTs) have gained great interest because of their unique properties such as high charge-carrier mobility, remarkable thermal conductivity, and large surface-area-to-volume ratio.[1−11] Various methods have been developed to integrate CNTs with graphene to form new hybrid materials. For example, the combination of graphene oxide and CNTs has been demonstrated to be high-performance, flexible, and transparent materials such as conductors, electrodes, and supercapacitors.[12−14] Metal catalysts such as copper or iron nanoparticles have been deposited onto graphene for the out-of-plane growth of CNTs through chemical vapor deposition (CVD).[15,16] Multi-walled CNT (MWNT)−graphene hybrids have exhibited an improved conductivity/transparency characteristic, in comparison with pure graphene and MWNTs, because of their very high aspect ratio and "glue" connections.[17] Moreover, veinlike MWNT network layers have been stacked to graphene to improve its mechanical strength.[18] However, the thickness of such hybrids ranges from 200 nm to a few microns, leading to a lower transparency (∼53% at 600 nm) than that of monolayer graphene (97.7% at 600 nm).[19] Recent studies also show that single-walled CNT (SWNT) networks on copper substrates can partially unzip into graphene nanoribbons through hydrogen annealing.[20] Although the applications of partially unzipped SWNT networks (rebar graphene) may be limited by their porous structures, rebar graphene can float on water and be transferred onto arbitrary substrates without a supporting layer, making it an ideal candidate for framing monolayer graphene to enhance its mechanical properties. Therefore, it is desirable to integrate SWNT networks with monolayer graphene to produce ultrathin SWNT−graphene films, which can inherit the unique optical and electrical properties from both graphene and SWNTs with improved mechanical strength.

Here, we introduce a simple method to synthesize ultrathin SWNT−graphene hybrid films. We first spin-coat a thin layer of SWNTs on a copper foil to form a supporting network frame and then introduce methane as a carbon feeding gas for monolayer graphene growth. Without utilizing the mechanical support from poly(methyl methacrylate) (PMMA), large-area SWNT−graphene hybrids can float on water and be transferred onto arbitrary substrates. Results from Raman spectroscopy and transmission electron microscopy (TEM) indicate that SWNT networks can connect different graphene grains together to form two-dimensional SWNT−graphene hybrids with a transparency as high as that of monolayer graphene. Electrical transport measurements show that SWNT−graphene hybrids maintain electrical properties similar to those of CVD-grown monolayer graphene, while exhibits a higher turn-on electrical conductance than SWNT networks alone. Scanning photocurrent measurements have also been utilized to investigate the local electrical conductivity of the hybrid materials. By comparing scanning photocurrent and scanning electron microscopy (SEM) images, we find that the interactions between SWNTs and graphene can induce photocurrent signals

Received: November 25, 2014
Accepted: February 16, 2015
Published: February 16, 2015

DOI: 10.1021/am5082843
ACS Appl. Mater. Interfaces 2015, 7, 5233−5238

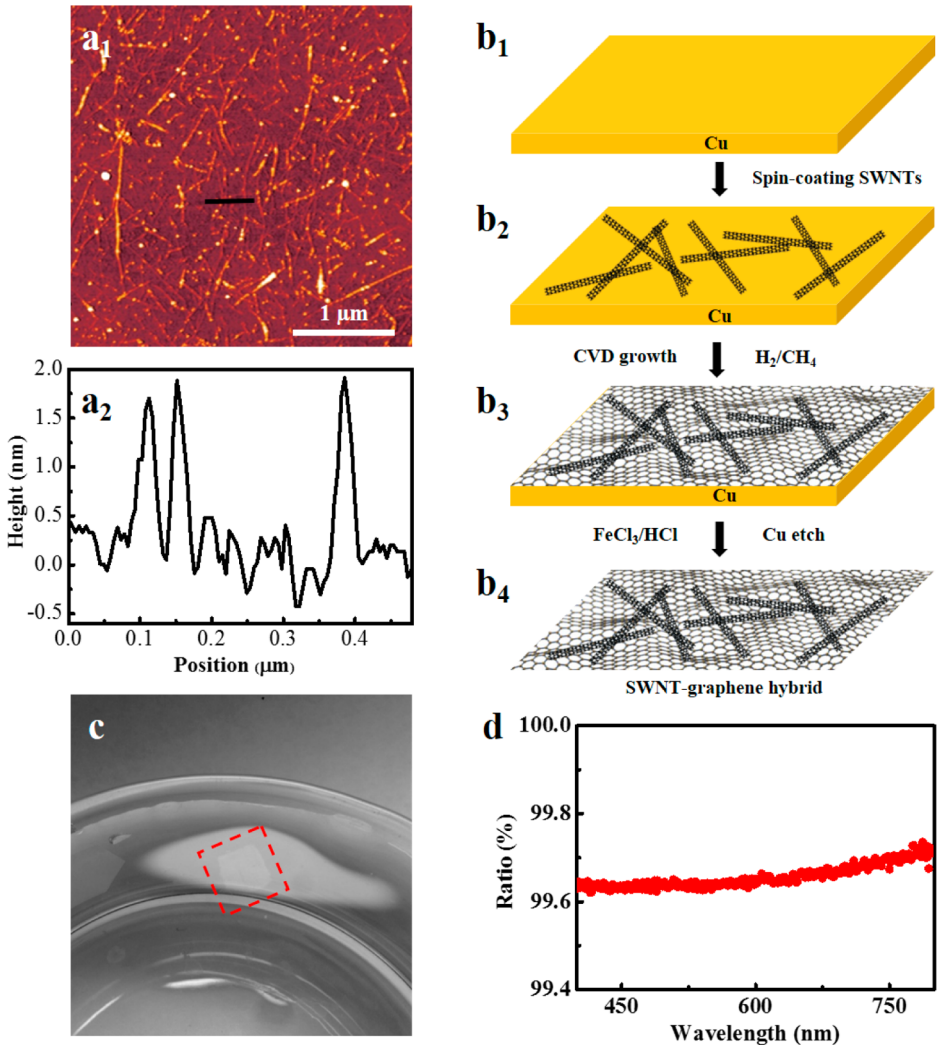

Figure 1. (a_1) Atomic force microscopy image of a SWNT network on a SiO_2/Si substrate. (a_2) Height profile of SWNTs along the black line in part a_1. (b) Schematic diagram of the synthesis process of SWNT−graphene hybrids. (c) Photograph of polymer-free SWNT−graphene hybrids floating on water. The red dashed square marks the location of the SWNT−graphene hybrids. (d) Light transmission ratio of SWNT−graphene hybrids to graphene in the visible regime.

in the junction regions of different graphene grains, where SWNTs act as glues to link them together. This may offer a new way to manipulate the photocurrent response of SWNT−graphene hybrids by controlling the morphologies of the SWNT frames.

2. EXPERIMENTAL SECTION

2.1. SWNT−Graphene Hybrid Synthesis. As-produced high-pressure carbon monoxide (HiPco) SWNTs were functionalized via reductive alkylation using lithium and alkyl halides in liquid ammonia.[21] The functionalized SWNTs were resuspended in chloroform and spin-coated on targeted substrates (Figure $1a_1$) to form a thin layer of randomly distributed SWNT networks, whose morphology was characterized by a JEOL JSPM-5200 scanning probe microscope. The height of the functionalized SWNTs is ∼2 nm (Figure $1a_2$), which is higher than the typical diameter (∼1 nm) of as-produced HiPco SWNTs[22] because of the sidewall functional groups.[21]

In order to form SWNT−graphene hybrids, we adopted a standard CVD method that was developed to synthesize graphene.[23−25] Copper foils (Alfa Aesar, 0.025 mm, 99.8%) with a grain size of ∼100 μm were cut into squares of 1.5 cm length. The copper foils were pretreated in a 5% nitric acid bath for 1−2 min and then in a deionized water bath for 3 min twice to remove the oxide layer and surface contamination (Figure $1b_1$).[26] After that, 50 μL of a functionalized SWNT−chloroform solution was spin-coated on top of a copper foil square at 4000 rpm for 45 s (Figure $1b_2$). For comparison, a copper foil square with SWNTs and one without SWNTs were loaded onto a quartz boat simultaneously, which was then transferred to a horizontal furnace system by a magnetic bar.[27] After the system was pumped down to 10 mTorr, the temperature was raised to 1000 °C, and the samples were annealed in 50 sccm H_2 for 1 h to remove the surface functional groups of SWNTs. 10 sccm CH_4 was then added to conduct graphene synthesis for 30 min (Figure $1b_3$). The boat was quickly pulled out of the furnace by a magnetic bar and placed on the downstream of the quartz tube at room temperature when graphene growth was completed.

2.2. Optical Characterization. The optical transmittance of graphene and SWNT−graphene hybrid samples was obtained by a Varian Cary 5000 UV−vis−near-IR spectrophotometer over a wavelength from 400 to 800 nm. Raman spectra were collected at room temperature through a Thermo Scientific DXR Raman spectrometer from 100 to 3000 cm^{-1}. A 532 nm laser beam was focused into a diffraction-limit laser spot (<1 μm) by a 100× Olympus objective for Raman spectroscopy. A total of 10 spots were randomly selected in each sample.

DOI: 10.1021/am5082843
ACS Appl. Mater. Interfaces 2015, 7, 5233−5238

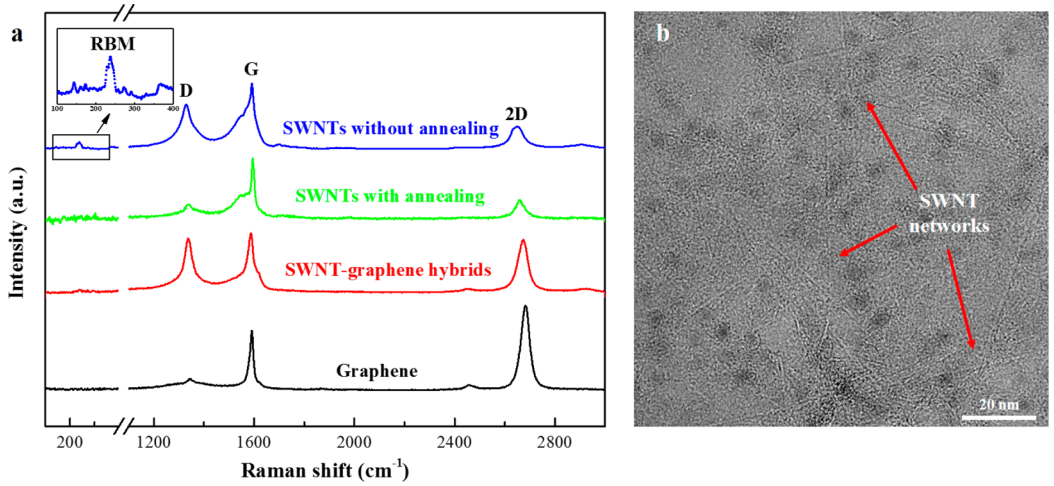

Figure 2. (a) Raman spectra of SWNT networks before (blue) and after (green) hydrogen annealing, SWNT−graphene hybrids (red), and monolayer graphene (black). Inset: Detailed spectrum of RBM for SWNT networks before annealing. (b) TEM image of SWNT−graphene hybrids showing that graphene is framed by SWNT networks, where SWNTs are marked by red arrows.

2.3. TEM and SEM Imaging. As-grown SWNT−graphene hybrids were directly transferred onto TEM grids coated with lacey carbon films, which were fixed on a clean glass coverslip by a small-volume drop of ethanol. The samples were then annealed in 100 sccm Ar and 10 sccm H_2 (under 10 m Torr chamber pressure) at 350 °C for 30 min to remove the amorphous carbon on the surface. Bright-field TEM imaging was performed on an FEI Tecnai Osiris transmission electron microscope operated at 200 kV. No obvious damage or structural transformation was observed on the hybrids under this voltage condition. The SEM images of SWNT−graphene hybrids were taken by a Raith eLINE system at 5 kV with a working distance of 10 mm.

2.4. Electrical Transport Measurements. SWNT networks, SWNT−graphene hybrids, and graphene were transferred onto prepatterned substrates, where source and drain electrodes were deposited with 5 nm of chromium and 40 nm of gold by an e-beam evaporator. For gate-dependent measurements, a gold wire was inserted into an 8-mm-diameter cylinder that was attached to the substrate and filled with a 1× phosphate-buffered saline (PBS) solution (~150 mM) to act as an electrolyte gate.

2.5. Scanning Photocurrent Microscopy. We performed spatially resolved scanning photocurrent measurements in an Olympus microscope setup. A continuous-wave laser source (λ = 785 nm) was expanded and altered by a nanometer-resolution scan mirror. The laser beam was then focused by a 40× objective (N.A. = 0.6) into a diffraction-limited spot (~1 μm) on the samples. The photocurrent signals were obtained using a preamplifier with the highest sensitivity within the measurement range. The reflection image was simultaneously recorded by a silicon detector. By overlapping the reflection image with the photocurrent image, the position of the sample was located.

3. RESULTS AND DISCUSSION

3.1. Mechanical Strength and Optical Transmittance Comparison. During the subsequent transfer process, the as-produced SWNT−graphene hybrid can withstand the surface tension and float on the surface of the copper etchant ($FeCl_3$) solution by itself (Figure 1c), while graphene synthesized during the same process needs the assistance of a PMMA layer. After the wet etching process with a $FeCl_3$ solution, we transferred the samples to a hydrochloric acid bath and then a deionized water bath several times to remove copper and chemical residues produced during the transfer (Figure 1b$_4$). The final films were transferred to glass coverslips for optical transmittance measurements. The light transmission of SWNT−graphene hybrids is as high as that of monolayer graphene, with less than 1% difference, as shown in Figure 1d.

3.2. Raman Spectroscopy and TEM Characterization. Raman spectroscopy was performed to characterize original SWNT networks, SWNT networks after hydrogen annealing, SWNT−graphene hybrids, and graphene on SiO_2/Si substrates (Figure 2a). For SWNT networks before hydrogen annealing, four typical strong bands were observed (Figures 2a, blue, and S1 in the Supporting Information): a diameter-dependent radial breathing mode (RBM) ranging from 225 to 275 cm^{-1}, a disorder mode (D) at ~1330 cm^{-1}, a tangential mode (G) at ~1590 cm^{-1}, and a 2D mode at ~2680 cm^{-1}. According to the ω_{RBM} (cm^{-1}) = 234/d_t (nm) + 10 relationship,[28,29] we obtain the diameter of randomly distributed SWNTs as ~0.9−1.1 nm, a typical diameter distribution of as-produced HiPco SWNTs.[22] A strong disorder band at ~1330 cm^{-1} shows up because of the covalent surface functionalization.[21]

In order to characterize SWNT networks after hydrogen annealing, SWNTs were first spin-coated on a copper foil, annealed in 50 sccm H_2 at 1000 °C for 1 h, and then followed the procedure described in the previous section to be transferred onto a Si/SiO_2 substrate (Figure 2b, green). After hydrogen annealing, the intensity of the D peak is significantly reduced because the functional groups are removed from SWNTs. A high tangential mode at 1590 cm^{-1} indicates that the graphitic structures survive during annealing. In addition, the RBM peak disappears in most locations and is only observed at 20 out of 100 randomly selected spots (Figure S2 in the Supporting Information), indicating that some SWNTs are partially unzipped through pure hydrogen annealing.[30] These are different from Raman spectra of rebar graphene reported in a previous study,[20] where the RBM peak is observed in the SWNT samples after annealing. One possible reason is that the hydrogen partial pressure is lower and the annealing time is shorter in the previous study than the annealing parameters used in our experiments. This indicates that our annealing conditions are more favorable to unzip SWNTs.

The Raman spectrum of graphene grown on a clean copper foil square shows that the intensity of the 2D mode (~2680 cm^{-1}) is ~1.5 times as high as that of the G mode (Figure 2a, black), indicating that the as-produced graphene is mono-

DOI: 10.1021/am5082843
ACS Appl. Mater. Interfaces 2015, 7, 5233−5238

layer.[23] However, the intensity of the 2D mode of SWNT−graphene hybrids synthesized simultaneously is less than or equal to the G-mode intensity, a typical spectrum of few-layer graphene.[23] In addition, the relatively high D peak for SWNT−graphene hybrids (Figure 2a, red) might be related to the interactions between graphene and SWNTs. Moreover, these interactions may further quench the RBM in the hybrid. These are consistent with scanning photocurrent measurements in the following section.

The structures of SWNT−graphene hybrids were investigated by TEM. As shown in Figure 2b, randomly distributed SWNT networks interlace with each other and form a solid backbone to support the graphene layer and to enhance the connection between different graphene grains. This 2D hybrid film exhibits better mechanical strength than monolayer graphene because it can float on water and can be transferred onto any substrate without polymer supporting layers. Interestingly, there are a few black nanoparticles on the SWNT−graphene hybrid films, which may result from copper residues during the transfer process or iron catalysts in as-grown HiPco SWNTs. More experiments need to be performed to further clean SWNT−graphene hybrid films in the future.

3.3. Electrical Transport Measurements. Electrical transport measurements were also performed to characterize the electrical performance of SWNT networks, SWNT−graphene hybrids, and graphene, respectively. SWNTs were spin-coated at 4000 rpm for 45 s onto a glass substrate and then annealed with 100 sccm Ar and 10 sccm H_2 at 350 °C for 30 min to remove surface functional groups, while the other two samples were transferred onto prepatterned glass substrates after a wet etching process as described in the previous section. A gold wire was used as an electrolyte gate to modulate the electrochemical potential. When the gate voltage swept from 0 to 1.2 V, the conductance of different samples was recorded at a source-drain bias of 50 mV.

As shown in Figure 3, randomly distributed SWNT networks exhibit a predominately p-type behavior at a gate voltage of 0 V, a typical electrical transport behavior of SWNTs.[31] On the other hand, the SWNT−graphene hybrid device shows higher conductance than pure SWNT networks when turned on, suggesting that the conductance of SWNT networks has been improved by the introduction of graphene. When the conductance of the SWNT−graphene hybrids (Figure 3b) is compared with that of monolayer graphene synthesized simultaneously (Figure 3c), it is obvious that the SWNT−graphene hybrids inherit the electrical transport properties from monolayer graphene because they show similar Dirac points ($V_{Dirac} \sim 0.8$ V) and gate-dependent behavior.

3.4. Scanning Photocurrent Microscopy. While the electrical transport properties of SWNT−graphene hybrids and graphene are similar to those of a whole film, it is also interesting to explore the local conductance distribution in SWNT−graphene hybridized structures through scanning photocurrent microscopy. In our experiments, a 785 nm diffraction-limited laser spot (~1 μm) was scanned over a SWNT−graphene hybrid transistor by a piezo-controlled mirror with nanometer-scale spatial resolution. A photocurrent signal occurs wherever the SWNT−graphene hybrid electronic band structure bends: the built-in electric field separates the photoexcited electron and hole pairs and thus produces a current.[32,33] This current is measured as a function of the position, as shown in Figure 4a. Interestingly, strong photocurrent responses were observed in some areas between two electrodes of the SWNT−graphene hybrid device, while photocurrent signals were only detected at graphene−electrode junctions in a standard graphene transistor due to the Schottky-like barrier between graphene and metal electrodes.[34,35] Corresponding SEM images suggest that the photocurrent response is located at the junctions between different graphene grains, which are glued by SWNT networks (Figure 4b−d). Previous studies indicate that the interaction between stacked graphene can introduce a strong photocurrent response at the junction between stacked and monolayer graphene.[24,25,36,37] The strong photocurrent response in SWNT−graphene hybrids may also stem from the interaction between SWNTs and graphene, consistent with the relatively high D peak in the Raman spectra (Figure 2a). Although the overall electrical properties of SWNT−graphene hybrids will not be altered by introducing SWNT networks, the interaction between SWNTs and graphene can influence the optoelectronic properties of the hybrids. Therefore, controlling the morphologies of SWNT frames, such as aligned SWNT networks, may provide a new way to modulate the photocurrent response of SWNT−graphene hybrids.

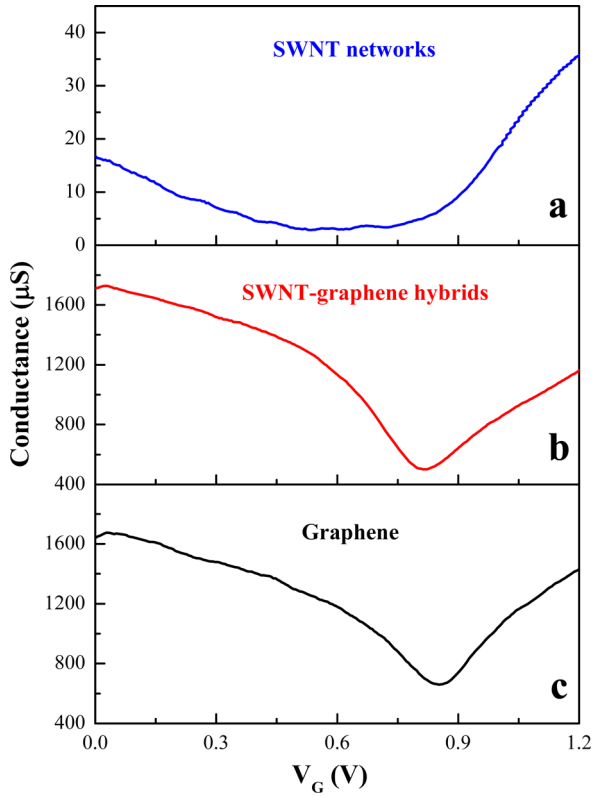

Figure 3. Gate-dependent measurements in (a) SWNT networks, (b) SWNT−graphene hybrids, and (c) monolayer graphene.

4. CONCLUSIONS

We develop a simple method to synthesize ultrathin SWNT−graphene hybrids, in which a thin layer of randomly distributed SWNT networks acts as a glue to connect different graphene grains together to improve their mechanical strength without degrading their high optical transmittance. Gate-dependent studies indicate that SWNT−graphene hybrids inherit the remarkable electrical properties from graphene and have higher turn-on conductance than the SWNT networks. Scanning

DOI: 10.1021/am5082843
ACS Appl. Mater. Interfaces 2015, 7, 5233−5238

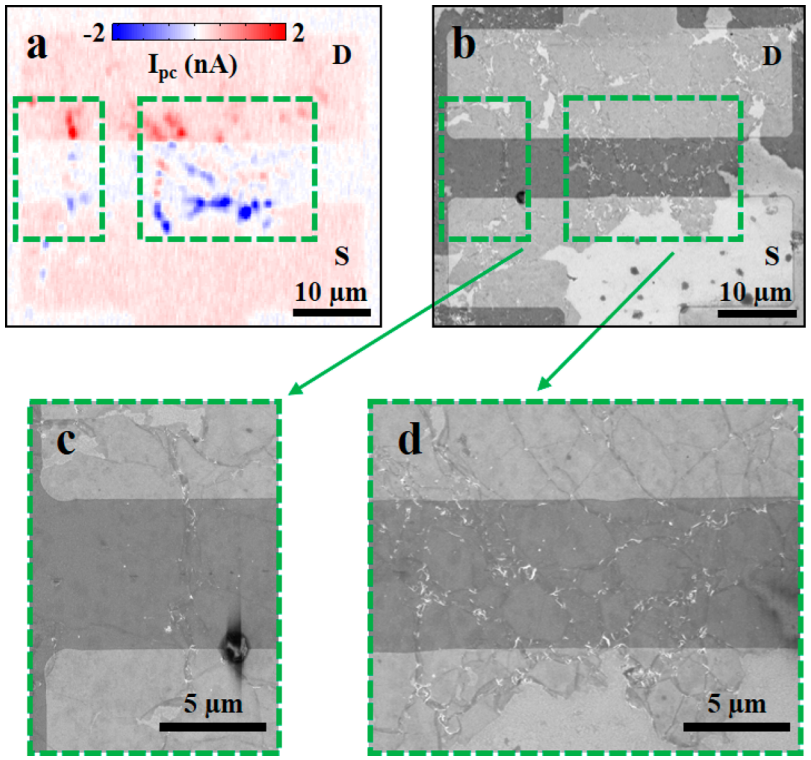

Figure 4. (a) Overlay of the photocurrent and reflection images of a SWNT−graphene hybrid transistor, (b) the corresponding SEM image, and (c and d) zoom-in SEM images of regions marked by green dashed rectangles in part b.

photocurrent measurements show that there are strong photocurrent signals at the junctions between different graphene grains, which may result from the interactions between graphene and SWNTs. The introduction of SWNT frames into graphene to enhance the linkage between different graphene grains and to engineer its photocurrent response may open a door for producing promising graphene hybrid structures for future applications in electronics and optoelectronics.

■ ASSOCIATED CONTENT

Supporting Information

Raman spectra. This material is available free of charge via the Internet at http://pubs.acs.org.

■ AUTHOR INFORMATION

Corresponding Author

*E-mail: yaqiong.xu@vanderbilt.edu.

Notes

The authors declare no competing financial interest.

■ ACKNOWLEDGMENTS

This work was supported by National Science Foundation Grants ECCE-1055852, CBET-1264982, and BIO-1450897. The devices were fabricated at the Cornell Nanoscale Science and Technology Facility and the Center for Nanophase Materials Sciences at the Oak Ridge National Laboratory.

■ REFERENCES

(1) Geim, A. K. Graphene: Status and Prospects. *Science* **2009**, *324* (5934), 1530−1534.
(2) Geim, A. K.; Novoselov, K. S. The rise of graphene. *Nat. Mater.* **2007**, *6* (3), 183−191.
(3) Bethune, D. S.; Kiang, C. H.; Devries, M. S.; Gorman, G.; Savoy, R.; Vazquez, J.; Beyers, R. Cobalt-Catalyzed Growth of Carbon Nanotubes with Single-Atomic-Layer walls. *Nature* **1993**, *363* (6430), 605−607.
(4) Iijima, S.; Ichihashi, T. Single-Shell Carbon Nanotubes of 1-nm Diameter. *Nature* **1993**, *364* (6439), 737−737.
(5) Novoselov, K. S.; Geim, A. K.; Morozov, S. V.; Jiang, D.; Katsnelson, M. I.; Grigorieva, I. V.; Dubonos, S. V.; Firsov, A. A. Two-dimensional gas of massless Dirac fermions in graphene. *Nature* **2005**, *438* (7065), 197−200.
(6) Novoselov, K. S.; Geim, A. K.; Morozov, S. V.; Jiang, D.; Zhang, Y.; Dubonos, S. V.; Grigorieva, I. V.; Firsov, A. A. Electric field effect in atomically thin carbon films. *Science* **2004**, *306* (5696), 666−9.
(7) Zhou, X. J.; Park, J. Y.; Huang, S. M.; Liu, J.; McEuen, P. L. Band structure, phonon scattering, and the performance limit of single-walled carbon nanotube transistors. *Phys. Rev. Lett.* **2005**, *95*, 146805.
(8) Bolotin, K. I.; Sikes, K. J.; Jiang, Z.; Klima, M.; Fudenberg, G.; Hone, J.; Kim, P.; Stormer, H. L. Ultrahigh electron mobility in suspended graphene. *Solid State Commun.* **2008**, *146* (9−10), 351−355.
(9) Balandin, A. A.; Ghosh, S.; Bao, W. Z.; Calizo, I.; Teweldebrhan, D.; Miao, F.; Lau, C. N. Superior thermal conductivity of single-layer graphene. *Nano Lett.* **2008**, *8* (3), 902−907.
(10) Pop, E.; Mann, D.; Wang, Q.; Goodson, K. E.; Dai, H. J. Thermal conductance of an individual single-wall carbon nanotube above room temperature. *Nano Lett.* **2006**, *6* (1), 96−100.
(11) Peigney, A.; Laurent, C.; Flahaut, E.; Bacsa, R. R.; Rousset, A. Specific surface area of carbon nanotubes and bundles of carbon nanotubes. *Carbon* **2001**, *39* (4), 507−514.
(12) Peng, L. W.; Feng, Y. Y.; Lv, P.; Lei, D.; Shen, Y. T.; Li, Y.; Feng, W. Transparent, Conductive, and Flexible Multiwalled Carbon Nanotube/Graphene Hybrid Electrodes with Two Three-Dimensional Microstructures. *J. Phys. Chem. C* **2012**, *116* (8), 4970−4978.
(13) Tung, V. C.; Chen, L. M.; Allen, M. J.; Wassei, J. K.; Nelson, K.; Kaner, R. B.; Yang, Y. Low-Temperature Solution Processing of Graphene−Carbon Nanotube Hybrid Materials for High-Performance Transparent Conductors. *Nano Lett.* **2009**, *9* (5), 1949−1955.

DOI: 10.1021/am5082843
ACS Appl. Mater. Interfaces 2015, 7, 5233−5238

(14) Hong, T. K.; Lee, D. W.; Choi, H. J.; Shin, H. S.; Kim, B. S. Transparent, Flexible Conducting Hybrid Multilayer Thin Films of Multiwalled Carbon Nanotubes with Graphene Nanosheets. *ACS Nano* **2010**, *4* (7), 3861−3868.
(15) Kim, Y. S.; Kumar, K.; Fisher, F. T.; Yang, E. H. Out-of-plane growth of CNTs on graphene for supercapacitor applications. *Nanotechnology* **2012**, *23*, 015301.
(16) Fan, Z. J.; Yan, J.; Zhi, L. J.; Zhang, Q.; Wei, T.; Feng, J.; Zhang, M. L.; Qian, W. Z.; Wei, F. A Three-Dimensional Carbon Nanotube/Graphene Sandwich and Its Application as Electrode in Supercapacitors. *Adv. Mater.* **2010**, *22* (33), 3723−+.
(17) Akilimali, R.; Macher, N.; Bonnefont, A.; Begin, D.; Janowska, I.; Pham-Huu, C. FLG-high aspect ratio MWNTs hybrid film prepared by hot spray technique. *Mater. Lett.* **2013**, *96*, 57−59.
(18) Lin, X. Y.; Liu, P.; Wei, Y.; Li, Q. Q.; Wang, J. P.; Wu, Y.; Feng, C.; Zhang, L. N.; Fan, S. S.; Jiang, K. L. Development of an ultra-thin film comprised of a graphene membrane and carbon nanotube vein support. *Nat. Commun.* **2013**, *4*, 2920.
(19) Nair, R. R.; Blake, P.; Grigorenko, A. N.; Novoselov, K. S.; Booth, T. J.; Stauber, T.; Peres, N. M. R.; Geim, A. K. Fine Structure Constant Defines Visual Transparency of Graphene. *Science* **2008**, *320* (5881), 1308.
(20) Yan, Z.; Peng, Z.; Casillas, G.; Lin, J.; Xiang, C.; Zhou, H.; Yang, Y.; Ruan, G.; Raji, A.-R. O.; Samuel, E. L. G.; Hauge, R. H.; Yacaman, M. J.; Tour, J. M. Rebar Graphene. *ACS Nano* **2014**, *8* (5), 5061−5068.
(21) Liang, F.; Sadana, A. K.; Peera, A.; Chattopadhyay, J.; Gu, Z.; Hauge, R. H.; Billups, W. E. A Convenient Route to Functionalized Carbon Nanotubes. *Nano Lett.* **2004**, *4* (7), 1257−1260.
(22) Nikolaev, P.; Bronikowski, M. J.; Bradley, R. K.; Rohmund, F.; Colbert, D. T.; Smith, K. A.; Smalley, R. E. Gas-phase catalytic growth of single-walled carbon nanotubes from carbon monoxide. *Chem. Phys. Lett.* **1999**, *313* (1−2), 91−97.
(23) Li, X. S.; Cai, W. W.; An, J. H.; Kim, S.; Nah, J.; Yang, D. X.; Piner, R.; Velamakanni, A.; Jung, I.; Tutuc, E.; Banerjee, S. K.; Colombo, L.; Ruoff, R. S. Large-Area Synthesis of High-Quality and Uniform Graphene Films on Copper Foils. *Science* **2009**, *324* (5932), 1312−1314.
(24) Jarrahi, Z.; Cao, Y.; Hong, T.; Puzyrev, Y.; Wang, B.; Lin, J.; Huffstutter, A.; Pantelides, S. T.; Xu, Y. Enhanced Photoresponse in Curled Graphene Ribbons. *Nanoscale* **2013**.
(25) Cao, Y. H.; Flores, R. L.; Xu, Y. Q. Curling graphene ribbons through thermal annealing. *Appl. Phys. Lett.* **2013**, *103*, 183103.
(26) Kim, S. M.; Hsu, A.; Lee, Y. H.; Dresselhaus, M.; Palacios, T.; Kim, K. K.; Kong, J. The effect of copper pre-cleaning on graphene synthesis. *Nanotechnology* **2013**, *24*, 365602.
(27) Xu, Y. Q.; Flor, E.; Kim, M. J.; Hamadani, B.; Schmidt, H.; Smalley, R. E.; Hauge, R. H. Vertical array growth of small diameter single-walled carbon nanotubes. *J. Am. Chem. Soc.* **2006**, *128* (20), 6560−6561.
(28) Fantini, C.; Jorio, A.; Souza, M.; Strano, M. S.; Dresselhaus, M. S.; Pimenta, M. A. Optical transition energies for carbon nanotubes from resonant Raman spectroscopy: Environment and temperature effects. *Phys. Rev. Lett.* **2004**, *93*, 147406-1.
(29) Souza, A. G.; Chou, S. G.; Samsonidze, G. G.; Dresselhaus, G.; Dresselhaus, M. S.; An, L.; Liu, J.; Swan, A. K.; Unlu, M. S.; Goldberg, B. B.; Jorio, A.; Gruneis, A.; Saito, R. Stokes and anti-Stokes Raman spectra of small-diameter isolated carbon nanotubes. *Phys. Rev. B* **2004**, *69*, 115428.
(30) Tsetseris, L.; Pantelides, S. T. Graphene nano-ribbon formation through hydrogen-induced unzipping of carbon nanotubes. *Appl. Phys. Lett.* **2011**, *99*, 143119.
(31) Avouris, P.; Chen, Z. H.; Perebeinos, V. Carbon-based electronics. *Nat. Nanotechnol.* **2007**, *2* (10), 605−615.
(32) Avouris, P. Carbon nanotube electronics and photonics. *Phys. Today* **2009**, *62* (1), 34−40.
(33) Avouris, P.; Freitag, M.; Perebeinos, V. Carbon-nanotube photonics and optoelectronics. *Nat. Photonics* **2008**, *2* (6), 341−350.
(34) Avouris, P. Graphene: Electronic and Photonic Properties and Devices. *Nano Lett.* **2010**, *10* (11), 4285−4294.
(35) Bonaccorso, F.; Sun, Z.; Hasan, T.; Ferrari, A. C. Graphene photonics and optoelectronics. *Nat. Photonics* **2010**, *4* (9), 611−622.
(36) Hong, T.; Cao, Y.; Ying, D.; Xu, Y.-Q. Thermal and optical properties of freestanding flat and stacked single-layer graphene in aqueous media. *Appl. Phys. Lett.* **2014**, *104* (22), 223102.
(37) Xu, X. D.; Gabor, N. M.; Alden, J. S.; van der Zande, A. M.; McEuen, P. L. Photo-Thermoelectric Effect at a Graphene Interface Junction. *Nano Lett.* **2010**, *10* (2), 562−566.

DOI: 10.1021/am5082843
ACS Appl. Mater. Interfaces 2015, 7, 5233−5238